PHYSICS LETTERS B

The $Z\gamma$ transverse-momentum spectrum at NNLO+N³LL

Marius Wiesemann [a],*, Luca Rottoli [b,c], Paolo Torrielli [d]

[a] *Max-Planck-Institut für Physik, Föhringer Ring 6, 80805 München, Germany*
[b] *Dipartimento di Fisica G. Occhialini, Università degli Studi di Milano-Bicocca and INFN, Piazza della Scienza 3, 20126 Milano, Italy*
[c] *Ernest Orlando Lawrence Berkeley National Laboratory, University of California, Berkeley, CA 94720, USA*
[d] *Dipartimento di Fisica and Arnold-Regge Center, Università di Torino and INFN, Sezione di Torino, Via P. Giuria 1, I-10125, Turin, Italy*

ARTICLE INFO

ABSTRACT

We consider the transverse-momentum (p_T) distribution of $Z\gamma$ pairs produced in hadronic collisions. Logarithmically enhanced contributions at small p_T are resummed to all orders in QCD perturbation theory and combined with the fixed-order prediction. We achieve the most advanced prediction for the $Z\gamma$ p_T spectrum by matching next-to-next-to-next-to-leading logarithmic (N³LL) resummation to the integrated cross section at next-to-next-to-leading order (NNLO). By considering $\ell^+\ell^-\gamma$ production at the fully differential level, including spin correlations, interferences and off-shell effects, arbitrary cuts can be applied to the leptons and the photon. We present results at the LHC in presence of fiducial cuts and find agreement with the 13 TeV ATLAS data at the few-percent level.

Vector-boson pair production processes are an integral part of the rich physics programme at the Large Hadron Collider (LHC). They play a crucial role in both precision measurements of Standard-Model (SM) rates and the search for new-physics phenomena. In particular, production processes of neutral vector bosons, like $Z\gamma$ production, provide very clean experimental signatures in the $Z \to \ell^+\ell^-$ decay channels, since the final state can be fully reconstructed. Their pure experimental signatures and relatively large cross sections render them well suited to search for anomalous couplings. For instance, the measurement of a non-zero $ZZ\gamma$ coupling, which is absent in the SM, would be direct evidence of physics beyond the SM (BSM). $Z\gamma$ production contributes also as irreducible background to direct searches for BSM resonances and to Higgs boson measurements, see e.g. Ref. [1]. Although the decay into a $Z\gamma$ pair of the Higgs boson is a rare loop-induced process in the SM, new-physics extensions may significantly enhance this decay channel.

The precise knowledge of rates and distributions in $Z\gamma$ production provides a strong test of the gauge structure of electroweak (EW) interactions and the mechanism of EW symmetry breaking. Measurements of $Z\gamma$ production have been carried out at the LHC at 7 TeV [2–7], 8 TeV [8–11], and 13 TeV [12,13]. The latest measurement of Ref. [13] is the first diboson analysis to use the full

Run II data set and achieves remarkably small experimental uncertainties.

To match the precision achieved by the experiments a significant effort has been made to advance theoretical predictions for $Z\gamma$ production in the past years. The next-to-leading order (NLO) QCD cross section has been known for some time both for on-shell Z bosons [14] and including their leptonic decays [15]. The loop induced gluon-fusion contribution was the first contribution to the next-to-next-to-leading order (NNLO) QCD cross section to be computed [16–18]. In Ref. [19] the NLO cross section, including photon radiation off the leptons, and the loop-induced gluon fusion contribution were combined. The complete NNLO QCD corrections to $\ell^+\ell^-\gamma$ production at the fully differential level were first calculated in Refs. [20,21] and later confirmed by an independent calculation [22]. Electroweak (EW) corrections were presented in Refs. [23,24].

Two different mechanisms are relevant to produce isolated photons in the final state: a perturbative one through *direct* production in the underlying hard subprocess, and a non-perturbative one through *fragmentation* of a quark or a gluon. The latter production mechanism requires the knowledge of the respective fragmentation functions to absorb singularities related to collinear photon emissions, and those functions are determined from data with relatively large uncertainties. In experimental analyses the fragmentation component is typically suppressed by the criteria used to isolate photons. On the theoretical side, the separation between the two production mechanisms is delicate, as sharply isolating the
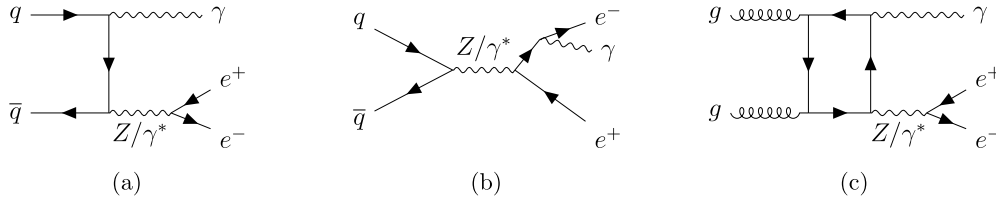
Fig. 1. Feynman diagrams for the production of two charged leptons and a photon: (a-b) sample tree-level diagrams in the quark-annihilation channel contributing at LO; (c) sample loop-induced diagram in the gluon-fusion channel contributing at NNLO.

photon from the partons would spoil infrared (IR) safety. Remarkably, by exploiting Frixione smooth-cone photon isolation [25] the fragmentation component can be completely removed in an IR-safe manner, which has the further advantage of substantially simplifying theoretical calculations of photon processes beyond the leading order (LO). Experimentally, the finite granularity of the calorimeter prevents a complete implementation of the smooth-cone isolation. As a consequence, experimental analyses rely instead on isolation criteria with a fixed cone. To facilitate data–theory comparisons, the smooth-cone parameters are typically tuned in comparisons with calculations including fragmentation functions in order to mimic the fixed-cone isolation criteria of the experiments, see e.g. Ref. [26]. Due to the large scale separation between the photon energy and the hadronic energy within the isolation cone, the presence of isolation cuts induces potentially large non-global (NG) logarithms, whose resummation is known up to leading-logarithmic (LL) accuracy [27,28] (see also Ref. [29]).

In this paper we consider the transverse-momentum (p_T) distribution of $Z\gamma$ pairs. This distribution is among the most important differential observables in $Z\gamma$ production, and it has recently been measured at a precision of a few percent by using the full Run II data set [13]. For the first time, we perform transverse-momentum resummation of $Z\gamma$ pairs at next-to-next-to-next-to-leading logarithmic (N^{3}LL) accuracy and match it to the NNLO integrated cross section. To this end, we calculate the process $pp \to \ell^+\ell^-\gamma$ with off-shell effects and spin correlations by consistently including all resonant and non-resonant topologies. Our computation is fully differential in the momenta of the final-state leptons and the photon, which allows us to apply arbitrary fiducial cuts.

We employ the MATRIX+RADISH interface [30], which combines NNLO calculations within MATRIX [31,32] with the RADISH resummation formalism of Refs. [33–35]. All tree-level and one-loop amplitudes are evaluated with OPENLOOPS 2 [36–38]. At two-loop level we use the $q\bar{q} \to V\gamma$ amplitudes of Ref. [39]. NNLO accuracy is achieved by a fully general implementation of the q_T-subtraction formalism [40] within MATRIX. The NLO parts therein (for $Z\gamma$ and $Z\gamma$+1-jet) are calculated by MUNICH[1] [43], which uses the Catani–Seymour dipole subtraction method [44,45]. The MATRIX framework features NNLO QCD corrections to a large number of colour-singlet processes at hadron colliders. It has already been used to obtain several state-of-the-art NNLO QCD predictions [20,21,46–52],[2] and for massive diboson processes it has been extended to combine NNLO QCD with NLO EW corrections [58] and with NLO QCD corrections to the loop-induced gluon fusion contribution [59,60]. Through the recently implemented MATRIX+RADISH interface [30] it is now also possible to deal with the resummation of transverse observables such as the transverse momentum of the colour-singlet final state.

We consider the process

$$pp \to \ell^+\ell^-\gamma + X$$

for massless leptons $\ell \in \{e, \mu\}$. Although our calculation also applies to the process $pp \to \nu\bar{\nu}\gamma + X$, we do not consider it here, as the transverse momentum of the $Z\gamma$ pair in that case cannot be experimentally reconstructed. Representative LO diagrams are shown in Fig. 1(a-b). They are driven by quark annihilation in the initial state and involve single-resonant t-channel $Z\gamma$ production (panel (a)) and single-resonant s-channel Drell–Yan (DY) topologies (panel (b)). Fig. 1(c) shows a loop-induced diagram that is driven by gluon fusion in the initial state and enters the cross section at NNLO. The loop-induced gluon-fusion contribution is effectively only LO accurate and has Born kinematics. Therefore, it contributes trivially to the $Z\gamma$ transverse-momentum ($p_{T,\ell\ell\gamma}$) distribution. Furthermore, its contribution is rather small, being less than 10% of the NNLO corrections and well below 1% of the full $Z\gamma$ cross section at NNLO [31]. We thus refrain from including the loop-induced gluon-fusion contribution in our calculation.

The perturbative description of the $Z\gamma$ transverse-momentum spectrum at fixed order breaks down in kinematic regimes dominated by soft and collinear QCD radiation, i.e. at small $p_{T,\ell\ell\gamma}$, due to the presence of large logarithms $L = \ln(m_{\ell\ell\gamma}/p_{T,\ell\ell\gamma})$, with $m_{\ell\ell\gamma}$ being the invariant mass of the $Z\gamma$ pair. Over the last four decades, a variety of formalisms has been developed to perform the resummation of large logarithmic contributions in the transverse momentum p_T of colour-singlet processes [33,34,61–70]. We employ the RADISH formalism of Refs. [33–35] to resum the relevant logarithmic terms to all orders. The logarithmic accuracy is customarily defined in terms of the logarithm of the cumulative cross section $\ln\sigma(p_T)$. The dominant terms $\alpha_S^n L^{n+1}$ are referred to as leading logarithmic, terms of $\alpha_S^n L^n$ as next-to-leading logarithmic (NLL), terms of $\alpha_S^n L^{n-1}$ as next-to-next-to-leading logarithmic (NNLL), and so on. We perform the resummation of the $Z\gamma$ p_T spectrum up to N^{3}LL based on the formulæ presented in Ref. [34]. The resummation formalism has been implemented in the RADISH code for Higgs and Drell-Yan production. The application to more complex colour-singlet processes, such as $Z\gamma$ production, is achieved through the MATRIX+RADISH interface [30]. We note that the LL resummation of the loop-induced gluon-fusion contribution to the $Z\gamma$ cross section is formally of the same order as N^{3}LL corrections to the $q\bar{q}$ channel, and that both contributions can be treated completely independently. The proper treatment of the former would require to go beyond an effective LO+LL accuracy, by combining NLO QCD corrections to the loop-induced gluon-fusion contribution with NNLL resummation. Given its small numerical impact, we leave such study for future work.

In order for the theoretical prediction to be reliable over the entire spectrum, the resummation of large logarithms at small p_T must be combined with the fixed-order cross section, valid at high p_T. We consistently match N^{3}LL resummation for the $p_{T,\ell\ell\gamma}$ spectrum with NNLO corrections at the level of cumulative cross section, defined as ($\kappa = $ NNLO, N^{3}LL)

---

[1] The Monte Carlo program MUNICH features a general implementation of an efficient, multi-channel based phase-space integration and computes both NLO QCD and NLO EW [41,42] corrections to arbitrary SM processes.

[2] It was also used in the NNLO+NNLL computation of Ref. [53], and in the NNLOPS computations of Refs. [54–57].

Table 1
Definition of phase-space cuts.

inclusive setup for $pp \to \ell\ell'\gamma + X$, $\quad \ell, \ell' \in \{e, \mu\}$
$p_{T,\gamma} \geq 10\,\text{GeV}$, $\quad |\eta_\gamma| \leq 2.37$, $\quad m_{\ell\gamma} \geq 4\,\text{GeV}$, $\quad 66\,\text{GeV} \leq m_{\ell\ell} \leq 116\,\text{GeV}$, Frixione isolation with $n = 2$, $\delta_0 = 0.1$, and $\epsilon = 0.1$.
fiducial setup for $pp \to \ell\ell'\gamma + X$, $\quad \ell, \ell' \in \{e, \mu\}$; used in the ATLAS 13 TeV analysis of Ref. [13]
$p_{T,\ell_1} \geq 30\,\text{GeV}$, $\quad p_{T,\ell_2} \geq 25\,\text{GeV}$, $\quad |\eta_\ell| \leq 2.47$, $\quad m_{\ell\ell} \geq 40\,\text{GeV}$, $p_{T,\gamma} \geq 30\,\text{GeV}$, $\quad |\eta_\gamma| \leq 2.37$, $\quad m_{\ell\ell} + m_{\ell\ell\gamma} \geq 182\,\text{GeV}$, $\quad \Delta R_{\ell\gamma} > 0.4$, Frixione isolation with $n = 2$, $\delta_0 = 0.1$, and $\epsilon = 0.1$, $\quad p_T^{\text{cone0.2}}/p_{T,\gamma} < 0.07$.

$$\sigma_\kappa(p_{T,\ell\ell\gamma}^{\text{veto}}) \equiv \int_0^{p_{T,\ell\ell\gamma}^{\text{veto}}} \mathrm{d}p_{T,\ell\ell\gamma} \, \frac{\mathrm{d}\sigma_\kappa(p_{T,\ell\ell\gamma})}{\mathrm{d}p_{T,\ell\ell\gamma}} \,. \tag{1}$$

The cross sections should be understood as being fully differential in the Born phase space, which allows us to apply arbitrary IR-safe cuts on the kinematics of the leptons and the photon.

There is a certain level of freedom when defining matching procedures that differ from one another only by terms beyond the formal accuracy of the calculation. We study two different matching schemes. The first scheme we consider is a customary additive scheme, which at NNLO+N^{3}LL is defined as

$$\sigma_{\text{NNLO+N}^3\text{LL}}^{\text{add. match.}}(p_{T,\ell\ell\gamma}^{\text{veto}}) = \sigma_{\text{NNLO}}(p_{T,\ell\ell\gamma}^{\text{veto}}) - \left[\sigma_{\text{N}^3\text{LL}}(p_{T,\ell\ell\gamma}^{\text{veto}})\right]_{\text{NNLO}} + \sigma_{\text{N}^3\text{LL}}(p_{T,\ell\ell\gamma}^{\text{veto}}) \,. \tag{2}$$

The notation $[\ldots]_{\text{N}^k\text{LO}}$ is used to indicate that the expression inside the bracket is expanded in α_S and truncated at N^{k}LO. Thus, the second term corresponds to the expansion of the resummed cumulative cross section $\sigma_{\text{N}^3\text{LL}}(p_{T,\ell\ell\gamma}^{\text{veto}})$ up to NNLO, i.e. $\mathcal{O}(\alpha_S^2)$, which subtracts all logarithmically enhanced contributions at small $p_{T,\ell\ell\gamma}^{\text{veto}}$ from the fixed-order component. This term is necessary to render Eq. (2) finite in the $p_{T,\ell\ell\gamma}^{\text{veto}} \to 0$ limit and to remove the double counting between the first and the third term.

The second scheme we consider is a multiplicative scheme [71, 72], defined as

$$\sigma_{\text{NNLO+N}^3\text{LL}}^{\text{mult. match.}}(p_{T,\ell\ell\gamma}^{\text{veto}})$$
$$= \frac{\sigma_{\text{N}^3\text{LL}}(p_{T,\ell\ell\gamma}^{\text{veto}})}{\sigma_{\text{N}^3\text{LL}}^{\text{asym.}}} \left[\sigma_{\text{N}^3\text{LL}}^{\text{asym.}} \frac{\sigma_{\text{NNLO}}(p_{T,\ell\ell\gamma}^{\text{veto}})}{\left[\sigma_{\text{N}^3\text{LL}}(p_{T,\ell\ell\gamma}^{\text{veto}})\right]_{\text{NNLO}}}\right]_{\text{NNLO}} \,, \tag{3}$$

where $\sigma_{\text{N}^3\text{LL}}^{\text{asym.}}$ is the asymptotic ($p_{T,\ell\ell\gamma}^{\text{veto}} \to \infty$) limit of the resummed cross section. In the limit $p_{T,\ell\ell\gamma}^{\text{veto}} \to 0$, Eq. (3) yields the resummed prediction, while for $p_{T,\ell\ell\gamma}^{\text{veto}} \to \infty$ it reproduces the fixed-order result. The detailed matching formulæ for the multiplicative scheme are reported in appendix A of ref. [71]. Since in both matching schemes the cumulative cross section tends to σ_{NNLO} when $p_{T,\ell\ell\gamma}^{\text{veto}} \to \infty$, by construction the differential distribution fulfils the unitarity constraint, i.e. its integral yields the NNLO cross section.

We present predictions for the LHC at 13 TeV. The EW parameters are evaluated through the G_μ scheme by setting the EW coupling to $\alpha = \sqrt{2}\,G_F m_W^2 \left(1 - m_W^2/m_Z^2\right)/\pi$ and the mixing angle to $\cos\theta_W^2 = (m_W^2 - i\Gamma_W m_W)/(m_Z^2 - i\Gamma_Z m_Z)$, employing the complex-mass scheme [73] throughout. We choose the PDG [74] values for the input parameters: $G_F = 1.16639 \times 10^{-5}\,\text{GeV}^{-2}$, $m_W = 80.385\,\text{GeV}$, $\Gamma_W = 2.0854\,\text{GeV}$, $m_Z = 91.1876\,\text{GeV}$, $\Gamma_Z = 2.4952\,\text{GeV}$. For each perturbative order we use the corresponding set of $N_f = 5$ NNPDF3.0 [75] parton distributions with $\alpha_S(m_Z) =$ 0.118. The renormalization scale (μ_R) and the factorization scale (μ_F) are chosen dynamically as

$$\mu_R = \mu_F = \mu_0 \equiv \sqrt{m_{\ell\ell}^2 + p_{T,\gamma}^2} \,, \tag{4}$$

while the resummation scale (Q) is set to

$$Q = Q_0 \equiv \frac{1}{2} m_{\ell\gamma} \,. \tag{5}$$

Uncertainties from missing higher-order contributions are estimated from customary 7-point renormalization- and factorization-scale variations by a factor of two around μ_0 for $Q = Q_0$ with the constraint $0.5 \leq \mu_R/\mu_F \leq 2$, and by varying Q by a factor of two around Q_0 for $\mu_F = \mu_R = \mu_0$. The total scale uncertainty is evaluated as the envelope of the resulting nine variations. The resummation is turned off at high $p_{T,\ell\ell\gamma}$ by means of modified logarithms as defined in Ref. [34], with exponent $p = 4$. We have checked that our predictions have a negligible dependence on the value of p. Non-perturbative corrections have not been included in our results.

We study predictions for the $p_{T,\ell\ell\gamma}$ distribution in two setups that involve different phase-space selection cuts, defined in Table 1: The first is a loose selection that solely aims at preventing QED singularities, including transverse-momentum and rapidity requirements for the photon, a lower invariant mass cut on the lepton–photon system, a Z-mass window for the lepton pair, and Frixione smooth-cone isolation [25]. This setup will be referred to as "inclusive" in the following. The second setup corresponds to the fiducial selection of the 13 TeV ATLAS analysis of Ref. [13], which uses a tighter requirement for the transverse momentum of the photon, a lower invariant-mass cut on the lepton pair, transverse-momentum and rapidity requirements on the leading and subleading lepton, a lower bound for the sum of the invariant masses of the lepton pair and the $\ell\ell\gamma$ system, a lepton–photon separation in $\Delta R = \sqrt{\Delta\phi^2 + \Delta\eta^2}$, and a two-fold photon isolation: in addition to a Frixione isolation with a rather small cone, the transverse energy of hadrons collimated with the photon is required not to exceed a small fraction of its transverse momentum. In our parton-level calculation we define $p_T^{\text{cone0.2}}$ as the sum of the transverse momenta of all partons within a cone of $R = 0.2$ around the photon. The second setup is referred to as "fiducial" in the following. One should bear in mind that such isolation criteria induce NG logarithmic corrections, which we do not resum in our formalism. We will estimate their effect on the $p_{T,\ell\ell\gamma}$ spectrum below.

We start the discussion of our results by comparing the expansion of the resummation with the fixed-order spectrum at small $p_{T,\ell\ell\gamma}$ in Fig. 2, which provides a strong check of our calculation. The plots demonstrate at a remarkable precision that the expansion of the resummed cross section matches the fixed-order cross section at small transverse momenta both for the inclusive setup in panel (a) and (b) and the fiducial setup in panel (c) and (d). As can be seen from the lower frame in panel (a) and (c), the relative difference Δ_{rel} between the NNLO distribution and the NNLO expansion of the N^{3}LL distribution normalized to the latter (red solid
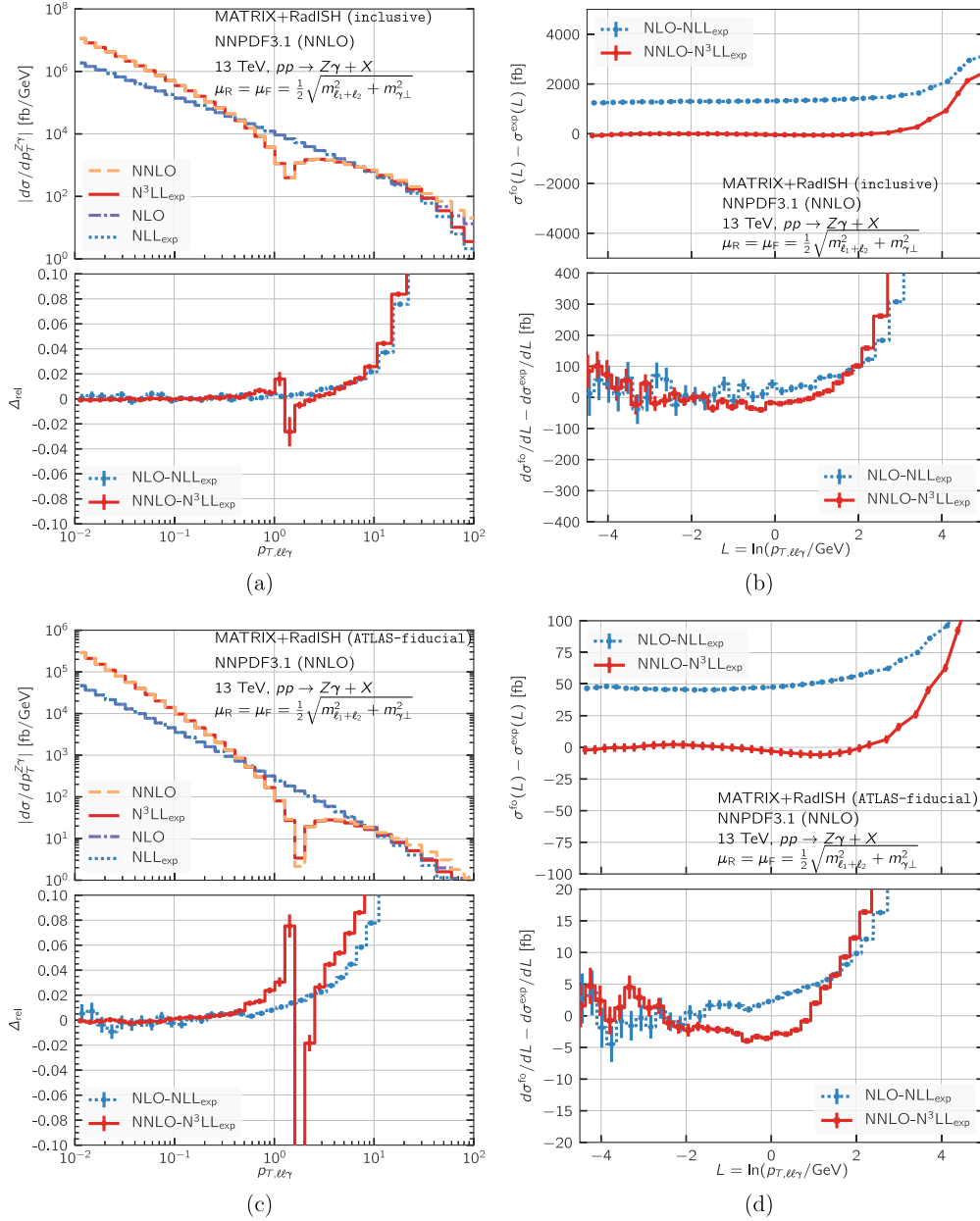
Fig. 2. Panel (a) and (c): transverse-momentum spectrum of the $Z\gamma$ pair at NLO (purple, dot-dashed) and NNLO (orange, dashed), and the expansion of the NLL (blue, dotted) and N^3LL (red, solid) cross section. The lower frame shows the relative difference between the fixed-order cross section and the expansion, normalized to the latter. Panel (b) and (d): the upper frame shows the difference at the cumulative level between NLO and NLL expansion (blue, dotted), and between NNLO and N^3LL expansion (red, solid). The lower frame shows the same results for the derivative of the cumulative cross section with respect to $\ln(p_{T,\ell\ell\gamma}/\text{GeV})$.

curve) vanishes down to $p_{T,\ell\ell\gamma} = 0.01$ GeV within the numerical errors at the permille level. In the upper frame of panel (b) and (d) we show the difference of the NNLO cross section and NNLO expansion of the N^3LL cross section at the cumulative level (red solid curve). Since their difference tends to zero at low transverse momenta, also constant terms in $p_{T,\ell\ell\gamma}$ match between NNLO and N^3LL. The fact that at NLO the difference with the NLL expansion (blue dotted curve) tends to a constant different from zero is expected, since our NLL result does not include the constant NLO terms in $p_{T,\ell\ell\gamma}$. Finally, the lower frame in panel (b) and (d) shows that the absolute difference between the fixed-order result and the expansion of the resummation after taking the derivative of the cumulative cross sections with respect to $\ln(p_{T,\ell\ell\gamma}/\text{GeV})$ yields zero within numerical uncertainties at small transverse momenta. This indicates that all logarithmic terms in $p_{T,\ell\ell\gamma}$ are correctly predicted. Not only do these comparisons provide stringent checks of

the validity of our calculation, but they also show the excellent precision that our numerical framework can achieve.

We further notice from these plots that the logarithmically enhanced contributions become dominant over the regular terms at smaller values of transverse momentum compared to other processes (cf. Ref. [30] for instance). Especially in the fiducial setup, regular contributions become non-negligible already at $p_{T,\ell\ell\gamma} \sim$ 1 GeV.[3] Indeed, it has been shown before [31,76] that processes with identified photons in the final state receive rather large corrections from power-suppressed terms at small transverse momen-

---

[3] We notice that the fiducial cuts used in Ref. [13] enhance u- and t-channel production modes, see Fig. 1 (a), while suppressing the s-channel contribution, see Fig. 1 (b). Therefore, the fiducial setup enhances power corrections stemming from non-singular gluon emission off the virtual quark propagator, see Fig. 1 (a).
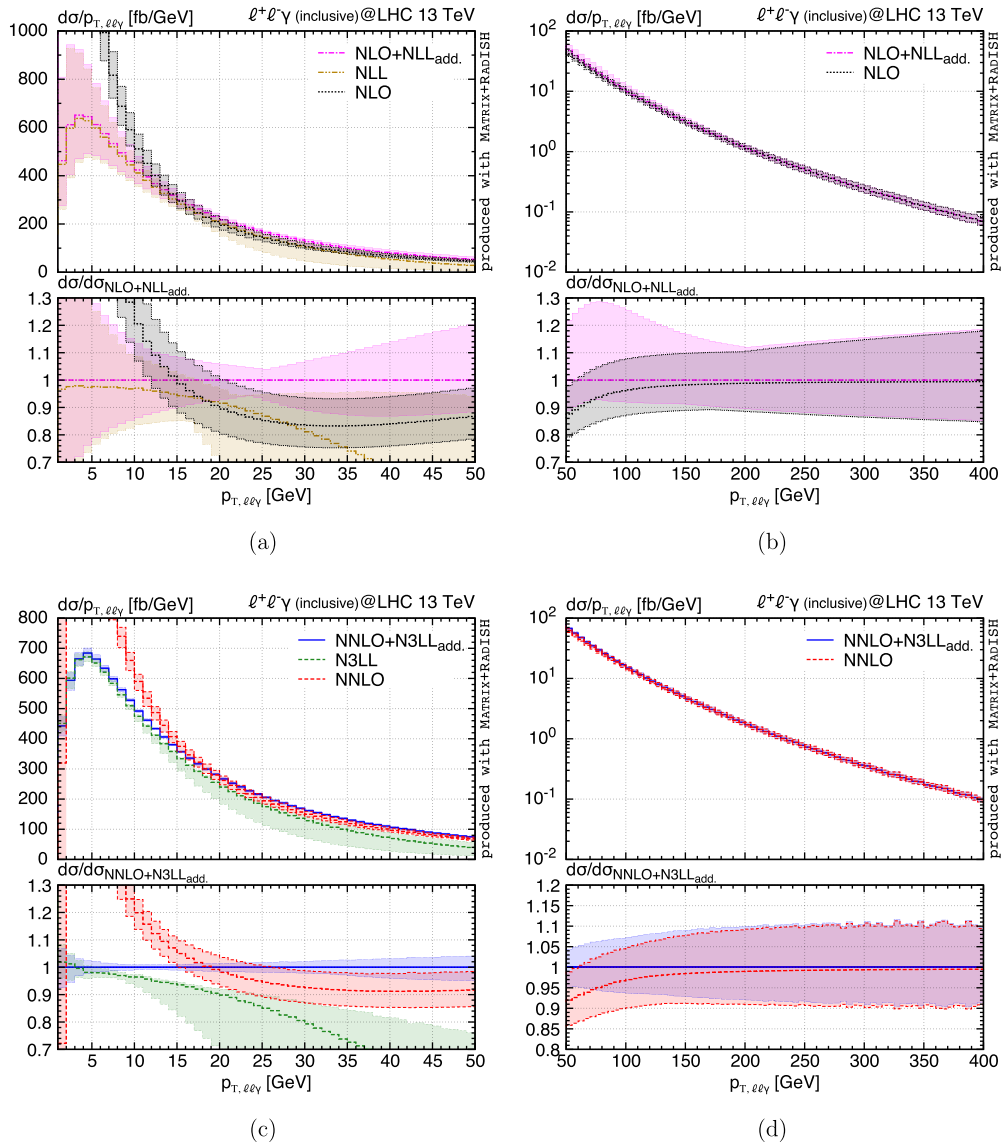
Fig. 3. Panel (a) and (b): $p_{T,\ell\ell\gamma}$ spectrum at NLO (black, dotted), NLL (brown, dash-double-dotted), and NLO+NLL (magenta, dash-dotted) in the small-$p_{T,\ell\ell\gamma}$ (panel (a)) and large-$p_{T,\ell\ell\gamma}$ (panel (b)) region. The lower frames show the ratio to the central NLO+NLL prediction. Panel (c) and (d): $p_{T,\ell\ell\gamma}$ spectrum at NNLO (red, dashed), N³LL (green, double-dash-dotted), and NNLO+N³LL (blue, solid) in the small-$p_{T,\ell\ell\gamma}$ (panel (a)) and large-$p_{T,\ell\ell\gamma}$ (panel (b)) region. The lower frames show the ratio to the central NNLO+N³LL prediction.

tum. In the multiplicative scheme Eq. (3) those are suppressed by $\sigma_{N^3LL}(p^{veto}_{T,\ell\ell\gamma})$ at small $p_{T,\ell\ell\gamma}$. Although such effects are beyond the nominal accuracy, this suppression may induce numerically relevant corrections, in particular in the fiducial setup considered here. This behaviour is undesirable, since on the one hand these power corrections are a genuine non-singular contribution to the cross section, and on the other hand the suppression of the latter induced by Eq. (3) is not the one dictated by an all-order resummation of such non-singular terms. For this reason we believe that the multiplicative scheme in Eq. (3), although formally correct, is not ideal when the fixed-order cross section features large power-suppressed corrections, and consequently we choose the additive scheme in Eq. (2) as the default throughout this paper.[4]

We now turn to discussing the resummed transverse-momentum spectrum of the $Z\gamma$ pair. Fig. 3 shows results in the inclusive setup and compares the matched NLO+NLL spectrum to the NLL and the NLO results in panel (a) and (b), and the matched NNLO+N³LL spectrum to the N³LL and the NNLO results in panel (c) and (d). At large transverse momenta (panel (b) and (d)), the matched results nicely converge towards the fixed-order predictions. At small transverse momenta (panel (a) and (c)), the NLO and NNLO predictions become unreliable, while the resummation yields physical results. The matched predictions are very close to the purely resummed ones at small transverse momenta and then progressively move farther apart at larger $p_{T,\ell\ell\gamma}$. Looking at the scale uncertainties, we observe a substantial reduction in the size of the respective bands when moving from NLO+NLL to NNLO+N³LL: At large $p_{T,\ell\ell\gamma}$ they decrease by roughly a factor of

---

[4] We point out that, although the multiplicative scheme in Eq. (3) (which is the default in MATRIX+RADISH) is suboptimal with respect to the additive scheme in Eq. (2) in cases where large power corrections are present, it should not be thought of as being suboptimal in general. In particular, for processes or setups where power corrections are moderate, their (undesirable) suppression, induced by the multiplicative matching, has very little impact on the physics results. Conversely a mul-

tiplicative matching is numerically more stable at small transverse momenta, and, more importantly, it includes the constant contributions in p_T through the matching when those are not available in the resummation component, cf. Refs. [30,71].
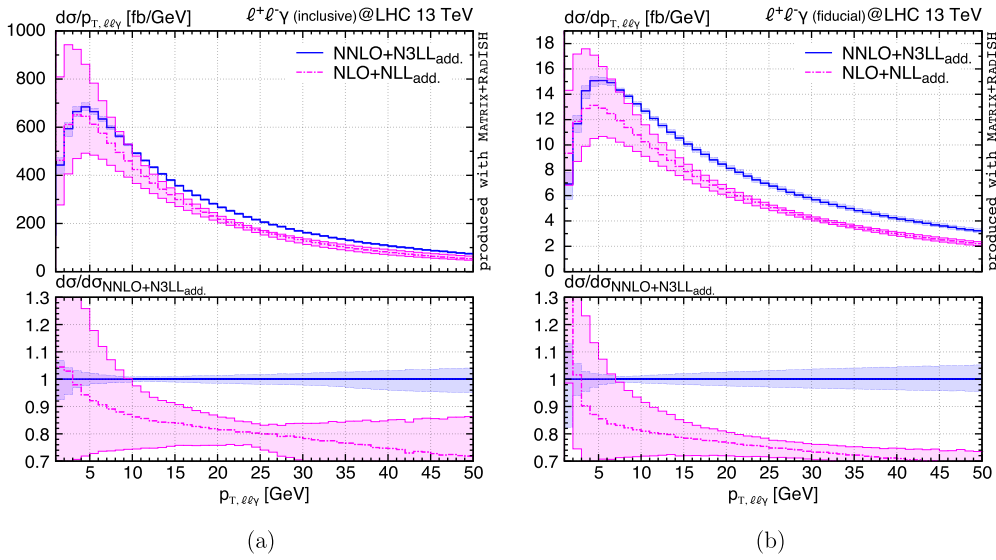
Fig. 4. $p_{T,\ell\ell\gamma}$ spectrum at NLO+NLL (magenta, dash-dotted) and NNLO+N^{3}LL (blue, solid) in the inclusive (panel (a)) and fiducial (panel (b)) setup. The lower frames show the ratio to the central NNLO+N^{3}LL prediction.

two, from 20% to 10%. At small $p_{T,\ell\ell\gamma}$ the reduction is even more significant. For $p_{T,\ell\ell\gamma} \lesssim 20$ GeV the NLO+NLL uncertainty increases between about 10% to more than 30%, while it is at the few-percent level at NNLO+N^{3}LL, reaching at most $\sim 8\%$ in the first bin.

Fig. 4 compares directly the results at NLO+NLL and NNLO+N^{3}LL at small transverse momenta, both in the inclusive setup in panel (a) and in the fiducial setup in panel (b). Higher-order corrections move the peak by 1–2 GeV towards larger values of $p_{T,\ell\ell\gamma}$. The substantial reduction of scale uncertainties has already been pointed out for the inclusive case, and we find a quite similar picture in the fiducial case. For $p_{T,\ell\ell\gamma} \lesssim 10$ GeV NLO+NLL and NNLO+N^{3}LL results agree within uncertainties with each other, although the corrections at $p_{T,\ell\ell\gamma} = 10$ GeV are already about 15% in both setups. With increasing values of $p_{T,\ell\ell\gamma}$ the corrections become progressively larger, reaching about 30% at $p_{T,\ell\ell\gamma} = 50$ GeV. For $p_{T,\ell\ell\gamma} \gtrsim 10$ GeV the higher-order corrections are not covered by the scale-uncertainty band of the NLO+NLL prediction, which appears to be significantly underestimated. This behaviour is not unexpected, as it is directly inherited from the fixed-order calculation, where the relatively small NLO uncertainties do not cover the substantial NNLO corrections in the tail. We stress that in the tail of the $p_{T,\ell\ell\gamma}$ distribution the (N)NLO prediction is effectively only (N)LO accurate, which explains this observation, as LO uncertainties generally tend to underestimate higher-order effects. While we find a fairly similar pattern in the two setups, the additional fiducial cuts tend to slightly increase the relative size of the corrections.

In Fig. 5 we compare our default NNLO+N^{3}LL predictions in the additive matching scheme of Eq. (2) with NNLO+N^{3}LL predictions in the multiplicative matching scheme of Eq. (3) for the inclusive case in panel (a) and (b), and for the fiducial case in panel (c) and (d). For large transverse momenta (panel (b) and (d)), the two predictions are in good agreement within uncertainties, since both eventually approach the NNLO result in the tail of the distribution. At small transverse momenta (panel (a) and (c)), the situation is different for the two setups. By and large, in the inclusive setup we find good agreement between the two matching schemes with overlapping uncertainty bands and at most 2% differences in the central value. The difference can be understood as an uncertainty related to the inclusion of terms beyond nominal accuracy in the matched prediction. In the fiducial setup the differences are somewhat larger. Multiplicative and additive schemes differ by up to

$\sim 8\%$ for $p_{T,\ell\ell\gamma}$ between 4 GeV and 20 GeV, and there is a gap between their uncertainty bands. This is in line with the large power corrections observed in the fiducial setup in Fig. 2 (c), which are suppressed in the multiplicative scheme and preserved in the additive one. As already stressed above, the suppression of such genuine non-singular contributions is undesirable, which justifies our preference for the additive scheme, especially in the fiducial setup, and we refrain from using the matching systematics as an additional uncertainty.

We continue by studying the impact of NG logarithmic terms stemming from photon isolation in Fig. 6. Such terms are not included in our resummation approach and enter only through the matching to fixed order. Fig. 6 (a) compares the NNLO+N^{3}LL predictions in the fiducial setup with and without the $p_T^{\text{cone0.2}}/p_{T,\gamma} < 0.07$ isolation cut (which is additional to the smooth-cone isolation). Their ratio indicates that at $p_{T,\ell\ell\gamma}$ values around the peak and smaller, the additional isolation has a minimal impact, as expected since it is power suppressed, while it induces effects of $\mathcal{O}(10\%)$ in the tail of the distribution. We show the same ratio at NNLO in the lower frame, which is essentially indistinguishable from the one at NNLO+N^{3}LL. In other words, isolation effects are adopted purely from the fixed-order prediction. In fact, the small effect at $p_{T,\ell\ell\gamma} \lesssim 10$ GeV indicates that the resummation of those corrections should have a minor impact in that region. Furthermore, we estimate the all-order effects of including NG logarithmic contributions in the fiducial setup using the PYTHIA8 [77] parton shower (PS) matched to NLO calculations in the MC@NLO scheme [78] within MADGRAPH5_AMC@NLO [79]. To this end, Fig. 6 (b) shows NLO+PS results with and without $p_T^{\text{cone0.2}}/p_{T,\gamma} < 0.07$ requirement in the main frame and their ratio in the lower frame. For comparison we show the same ratio at LO+PS and at NLO. The effects of the additional isolation are vanishingly small at LO+PS, which can be considered a lower bound for the impact that NG logarithmic terms stemming from photon isolation have on the all-order prediction of $p_{T,\ell\ell\gamma}$. The ratios at NLO+PS and at NLO are very similar to each other, with the matching to PS slightly reducing the effects due the additional isolation requirement. Their difference can be regarded as an estimate of the size of the NG logarithmic corrections beyond fixed order induced by the $p_T^{\text{cone0.2}}/p_{T,\gamma} < 0.07$ requirement. Since the difference is very small at low $p_{T,\ell\ell\gamma}$ and at most $\sim 2\%$ in the matching region, we neglect such effect from now on. We note that it is less straightforward to estimate the NG logarithmic contributions for the Frixione
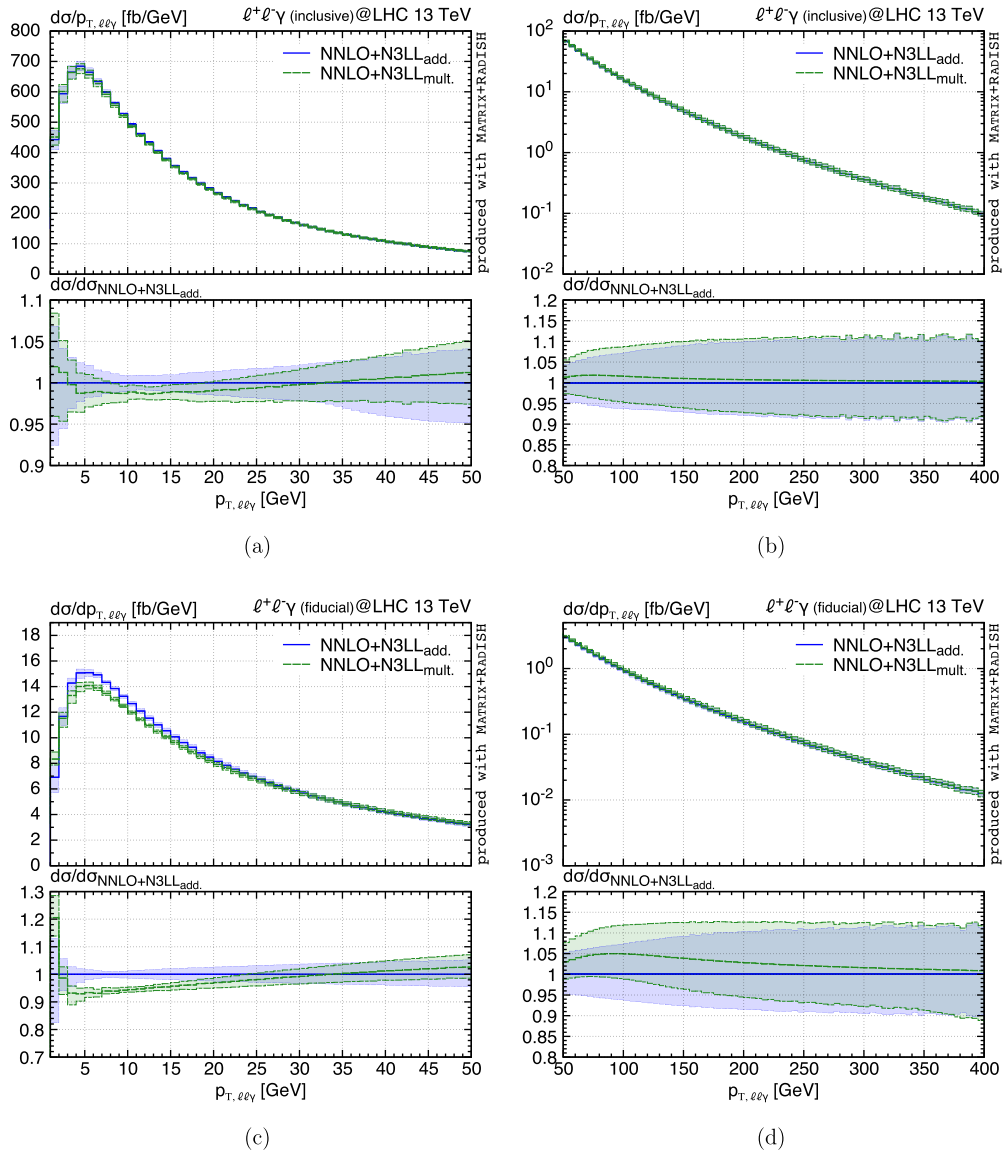
Fig. 5. $p_{T,\ell\ell\gamma}$ spectrum at NNLO+N^{3}LL in the additive matching scheme (blue, solid) and in the multiplicative matching scheme (green, long-dashed) in the inclusive (panel (a) and (b)) and fiducial (panel (c) and (d)) setup, showing the small-$p_{T,\ell\ell\gamma}$ (panel (a) and (c)) and large-$p_{T,\ell\ell\gamma}$ (panel (b) and (d)) region. The lower frames show the ratio to the central prediction in the additive scheme.

smooth-cone isolation, which for IR safety cannot be removed. However, we have verified that by varying the smooth-cone radius down to $\delta_0 = 0.01$ the analogous difference is only moderately affected and remains negligible at and below the peak of the spectrum.

We conclude our analysis by comparing our NNLO+N^{3}LL predictions to 13 TeV ATLAS data [13] in Fig. 7. The analysis of Ref. [13] is the first diboson measurement that includes the full Run II data set. The agreement is truly remarkable, especially with the precision of both theoretical prediction and data being at the few-percent level. The shape of the distribution is very well described by the predicted spectrum, and none of the data points are more than one standard deviation away from the theoretical uncertainty band. We observe that resummation and matching are crucial not only at small $p_{T,\ell\ell\gamma}$, but also in the intermediate region $40 \lesssim p_{T,\ell\ell\gamma} \lesssim 200$ GeV, where the comparison to data is significantly improved with respect to the NNLO comparison carried out in Ref. [13]. Furthermore, our results are a clear improvement over the comparison against NLO+PS predictions in Ref. [13]. In conclusion, our resummed results not only constitute the most precise

prediction of the spectrum to date, but they also provide the most accurate description of the 13 TeV ATLAS data.

To summarize, we have presented the first calculation of the transverse-momentum spectrum of $Z\gamma$ pairs at NNLO+N^{3}LL. At high transverse momenta we exploit the most accurate fixed-order prediction known to date, while at small transverse momenta we perform transverse-momentum resummation at N^{3}LL accuracy for the first time. Furthermore, our matching approach respects the unitarity of the spectrum, so that its integral yields exactly the total cross section at NNLO. Our results show that higher-order corrections in both the fixed-order and the logarithmic series are mandatory to obtain a reliable description of the distribution. Comparing NLO+NLL to NNLO+N^{3}LL predictions we find corrections of more than 30% in the tail of the distribution both in our inclusive and our fiducial setup. Those are inherited directly from the large NNLO corrections. Around the peak of the spectrum, we find corrections between 10% and 20% with a clear change in shape of the distribution. Moreover, at NNLO+N^{3}LL the peak moves by 1–2 GeV towards larger transverse momenta with respect to NLO+NLL. The inclusion of higher-order corrections substantially
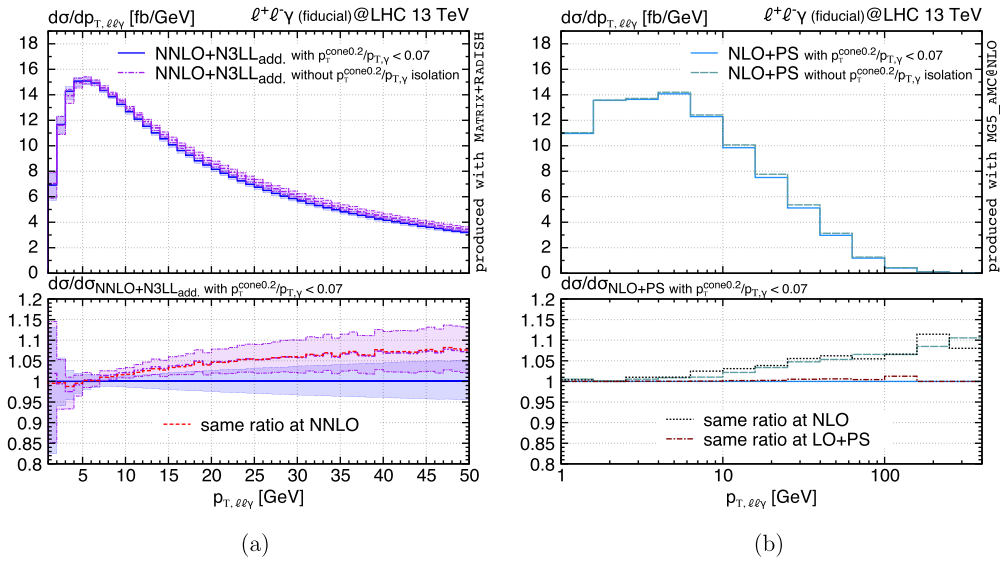
Fig. 6. Panel (a): $p_{T,\ell\ell\gamma}$ spectrum at NNLO+N^{3}LL in the fiducial setup (blue, solid) and without the additional $p_T^{cone0.2}/p_{T,\gamma}$ isolation (purple, dash-dotted). The lower frame shows the ratio to the central prediction with the $p_T^{cone0.2}/p_{T,\gamma} < 0.07$ requirement as well as the result when taking the same ratio for the central predictions at NNLO (red, dashed). Panel (b): Same results for central predictions at NLO+PS with $p_T^{cone0.2}/p_{T,\gamma} < 0.07$ requirement (light blue, solid) and without (grey-blue, long-dashed). The lower frame shows the ratio to the former as well as the same ratios at NLO (black, dotted) and at LO+PS (brown, dash-dotted).
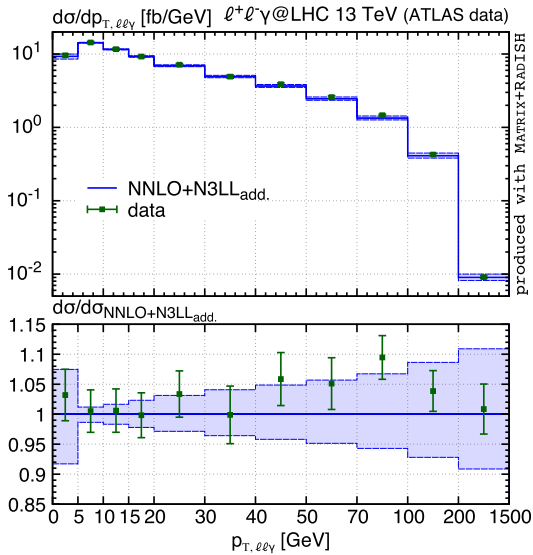

Fig. 7. NNLO+N^{3}LL prediction of the $p_{T,\ell\ell\gamma}$ spectrum (blue, solid) compared to AT-LAS data [13] (green data points). The lower frame shows the ratio to the central NNLO+N^{3}LL prediction.

reduces scale uncertainties, especially in the region of small transverse momenta. Furthermore, by means of an NLO+PS simulation we have estimated the impact of including NG logarithmic contributions beyond fixed order and found it to be minor with respect to the NNLO+N^{3}LL scale uncertainties. Finally, we have compared our best prediction at NNLO+N^{3}LL to ATLAS data at 13 TeV for the transverse-momentum spectrum of the $Z\gamma$ pair, and found a remarkable agreement within uncertainties at the few-percent level. We reckon that our results will play a crucial role in the rich physics programme that is based on precision studies of $Z\gamma$ production at the LHC.

Declaration of competing interest

None.

Acknowledgements

References

[1] G. Aad, et al., ATLAS, arXiv:2005.05382 [hep-ex], 2020.

[2] S. Chatrchyan, et al., CMS, Phys. Lett. B 701 (2011) 535, arXiv:1105.2758 [hep-ex].

[3] G. Aad, et al., ATLAS, J. High Energy Phys. 09 (2011) 072, arXiv:1106.1592 [hep-ex].

[4] G. Aad, et al., ATLAS, Phys. Lett. B 717 (2012) 49, arXiv:1205.2531 [hep-ex].

[5] S. Chatrchyan, et al., CMS, Phys. Rev. D 89 (2014) 092005, arXiv:1308.6832 [hep-ex].

[6] S. Chatrchyan, et al., CMS, J. High Energy Phys. 10 (2013) 164, arXiv:1309.1117 [hep-ex].

[7] G. Aad, et al., ATLAS, Phys. Rev. D 87 (2013) 112003, Erratum: Phys. Rev. D 91 (2015) 119901, arXiv:1302.1283 [hep-ex].

[8] G. Aad, et al., ATLAS, Phys. Lett. B 738 (2014) 428, arXiv:1407.8150 [hep-ex].

[9] V. Khachatryan, et al., CMS, J. High Energy Phys. 04 (2015) 164, arXiv:1502.05664 [hep-ex].

[10] V. Khachatryan, et al., CMS, Phys. Lett. B 760 (2016) 448, arXiv:1602.07152 [hep-ex].

[11] G. Aad, et al., ATLAS, Phys. Rev. D 93 (2016) 112002, arXiv:1604.05232 [hep-ex].

[12] M. Aaboud, et al., ATLAS, J. High Energy Phys. 12 (2018) 010, arXiv:1810.04995 [hep-ex].

[13] G. Aad, et al., ATLAS, J. High Energy Phys. 03 (2020) 054, arXiv:1911.04813 [hep-ex].

[14] J. Ohnemus, Phys. Rev. D 47 (1993) 940.

[15] U. Baur, T. Han, J. Ohnemus, Phys. Rev. D 57 (1998) 2823, arXiv:hep-ph/9710416.

[16] L. Ametller, E. Gava, N. Paver, D. Treleani, Phys. Rev. D 32 (1985) 1699.

[17] J. van der Bij, E. Glover, Phys. Lett. B 206 (1988) 701.

[18] K. Adamson, D. de Florian, A. Signer, Phys. Rev. D 67 (2003) 034016, arXiv:hep-ph/0211295.

[19] J.M. Campbell, R. Ellis, C. Williams, J. High Energy Phys. 07 (2011) 018, arXiv:1105.0020 [hep-ph].

[20] M. Grazzini, S. Kallweit, D. Rathlev, A. Torre, Phys. Lett. B 731 (2014) 204, arXiv:1309.7000 [hep-ph].

[21] M. Grazzini, S. Kallweit, D. Rathlev, J. High Energy Phys. 07 (2015) 085, arXiv:1504.01330 [hep-ph].

[22] J.M. Campbell, T. Neumann, C. Williams, J. High Energy Phys. 11 (2017) 150, arXiv:1708.02925 [hep-ph].
[23] W. Hollik, C. Meier, Phys. Lett. B 590 (2004) 69, arXiv:hep-ph/0402281.
[24] E. Accomando, A. Denner, C. Meier, Eur. Phys. J. C 47 (2006) 125, arXiv:hep-ph/0509234.
[25] S. Frixione, Phys. Lett. B 429 (1998) 369, arXiv:hep-ph/9801442.
[26] S. Catani, L. Cieri, D. de Florian, G. Ferrera, M. Grazzini, J. High Energy Phys. 04 (2018) 142, arXiv:1802.02095 [hep-ph].
[27] M. Dasgupta, G. Salam, Phys. Lett. B 512 (2001) 323, arXiv:hep-ph/0104277.
[28] M. Balsiger, T. Becher, D.Y. Shao, J. High Energy Phys. 08 (2018) 104, arXiv:1803.07045 [hep-ph].
[29] S. Catani, M. Fontannaz, J. Guillet, E. Pilon, J. High Energy Phys. 09 (2013) 007, arXiv:1306.6498 [hep-ph].
[30] S. Kallweit, E. Re, L. Rottoli, M. Wiesemann, arXiv:2004.07720 [hep-ph].
[31] M. Grazzini, S. Kallweit, M. Wiesemann, Eur. Phys. J. C 78 (2018) 537, arXiv:1711.06631 [hep-ph].
[32] http://matrix.hepforge.org.
[33] P.F. Monni, E. Re, P. Torrielli, Phys. Rev. Lett. 116 (2016) 242001, arXiv:1604.02191 [hep-ph].
[34] W. Bizon, P.F. Monni, E. Re, L. Rottoli, P. Torrielli, J. High Energy Phys. 02 (2018) 108, arXiv:1705.09127 [hep-ph].
[35] P.F. Monni, L. Rottoli, P. Torrielli, arXiv:1909.04704 [hep-ph].
[36] F. Cascioli, P. Maierhöfer, S. Pozzorini, Phys. Rev. Lett. 108 (2012) 111601, arXiv:1111.5206 [hep-ph].
[37] F. Buccioni, S. Pozzorini, M. Zoller, Eur. Phys. J. C 78 (2018) 70, arXiv:1710.11452 [hep-ph].
[38] F. Buccioni, J.-N. Lang, J.M. Lindert, P. Maierhöfer, S. Pozzorini, H. Zhang, M.F. Zoller, Eur. Phys. J. C 79 (2019) 866, arXiv:1907.13071 [hep-ph].
[39] T. Gehrmann, L. Tancredi, J. High Energy Phys. 02 (2012) 004, arXiv:1112.1531 [hep-ph].
[40] S. Catani, M. Grazzini, Phys. Rev. Lett. 98 (2007) 222002, arXiv:hep-ph/0703012.
[41] S. Kallweit, J.M. Lindert, P. Maierhöfer, S. Pozzorini, M. Schönherr, J. High Energy Phys. 04 (2015) 012, arXiv:1412.5157 [hep-ph].
[42] S. Kallweit, J.M. Lindert, P. Maierhöfer, S. Pozzorini, M. Schönherr, J. High Energy Phys. 04 (2016) 021, arXiv:1511.08692 [hep-ph].
[43] Munich is the abbreviation of "MUlti-chaNnel Integrator at Swiss (CH) precision"—an automated parton level NLO generator by S. Kallweit, in preparation.
[44] S. Catani, M. Seymour, Phys. Lett. B 378 (1996) 287, arXiv:hep-ph/9602277.
[45] S. Catani, M. Seymour, Nucl. Phys. B 485 (1997) 291, arXiv:hep-ph/9605323.
[46] F. Cascioli, T. Gehrmann, M. Grazzini, S. Kallweit, P. Maierhöfer, A. von Manteuffel, S. Pozzorini, D. Rathlev, L. Tancredi, E. Weihs, Phys. Lett. B 735 (2014) 311, arXiv:1405.2219 [hep-ph].
[47] M. Grazzini, S. Kallweit, D. Rathlev, Phys. Lett. B 750 (2015) 407, arXiv:1507.06257 [hep-ph].
[48] T. Gehrmann, M. Grazzini, S. Kallweit, P. Maierhöfer, A. von Manteuffel, S. Pozzorini, D. Rathlev, L. Tancredi, Phys. Rev. Lett. 113 (2014) 212001, arXiv:1408.5243 [hep-ph].
[49] M. Grazzini, S. Kallweit, S. Pozzorini, D. Rathlev, M. Wiesemann, J. High Energy Phys. 08 (2016) 140, arXiv:1605.02716 [hep-ph].
[50] M. Grazzini, S. Kallweit, D. Rathlev, M. Wiesemann, Phys. Lett. B 761 (2016) 179, arXiv:1604.08576 [hep-ph].
[51] M. Grazzini, S. Kallweit, D. Rathlev, M. Wiesemann, J. High Energy Phys. 05 (2017) 139, arXiv:1703.09065 [hep-ph].
[52] S. Kallweit, M. Wiesemann, Phys. Lett. B 786 (2018) 382, arXiv:1806.05941 [hep-ph].
[53] M. Grazzini, S. Kallweit, D. Rathlev, M. Wiesemann, J. High Energy Phys. 08 (2015) 154, arXiv:1507.02565 [hep-ph].
[54] E. Re, M. Wiesemann, G. Zanderighi, J. High Energy Phys. 12 (2018) 121, arXiv:1805.09857 [hep-ph].
[55] P.F. Monni, P. Nason, E. Re, M. Wiesemann, G. Zanderighi, J. High Energy Phys. 05 (2020) 143, arXiv:1908.06987 [hep-ph].
[56] S. Alioli, A. Broggio, S. Kallweit, M.A. Lim, L. Rottoli, Phys. Rev. D 100 (2019) 096016, arXiv:1909.02026 [hep-ph].
[57] P.F. Monni, E. Re, M. Wiesemann, arXiv:2006.04133 [hep-ph].
[58] M. Grazzini, S. Kallweit, J.M. Lindert, S. Pozzorini, M. Wiesemann, J. High Energy Phys. 02 (2020) 087, arXiv:1912.00068 [hep-ph].
[59] M. Grazzini, S. Kallweit, M. Wiesemann, J.Y. Yook, J. High Energy Phys. 03 (2019) 070, arXiv:1811.09593 [hep-ph].
[60] M. Grazzini, S. Kallweit, M. Wiesemann, J.Y. Yook, Phys. Lett. B 804 (2020) 135399, arXiv:2002.01877 [hep-ph].
[61] G. Parisi, R. Petronzio, Nucl. Phys. B 154 (1979) 427.
[62] J.C. Collins, D.E. Soper, G.F. Sterman, Nucl. Phys. B 250 (1985) 199.
[63] A. Idilbi, X.-d. Ji, F. Yuan, Phys. Lett. B 625 (2005) 253, arXiv:hep-ph/0507196 [hep-ph].
[64] G. Bozzi, S. Catani, D. de Florian, M. Grazzini, Nucl. Phys. B 737 (2006) 73, arXiv:hep-ph/0508068.
[65] S. Catani, M. Grazzini, Nucl. Phys. B 845 (2011) 297, arXiv:1011.3918 [hep-ph].
[66] T. Becher, M. Neubert, Eur. Phys. J. C 71 (2011) 1665, arXiv:1007.4005 [hep-ph].
[67] T. Becher, M. Neubert, D. Wilhelm, J. High Energy Phys. 02 (2012) 124, arXiv:1109.6027 [hep-ph].
[68] M.G. Echevarria, A. Idilbi, I. Scimemi, J. High Energy Phys. 07 (2012) 002, arXiv:1111.4996 [hep-ph].
[69] J.-Y. Chiu, A. Jain, D. Neill, I.Z. Rothstein, J. High Energy Phys. 05 (2012) 084, arXiv:1202.0814 [hep-ph].
[70] M.A. Ebert, F.J. Tackmann, J. High Energy Phys. 02 (2017) 110, arXiv:1611.08610 [hep-ph].
[71] W. Bizon, X. Chen, A. Gehrmann-De Ridder, T. Gehrmann, N. Glover, A. Huss, P.F. Monni, E. Re, L. Rottoli, P. Torrielli, J. High Energy Phys. 12 (2018) 132, arXiv:1805.05916 [hep-ph].
[72] W. Bizon, A. Gehrmann-De Ridder, T. Gehrmann, N. Glover, A. Huss, P.F. Monni, E. Re, L. Rottoli, D.M. Walker, Eur. Phys. J. C 79 (2019) 868, arXiv:1905.05171 [hep-ph].
[73] A. Denner, S. Dittmaier, M. Roth, L.H. Wieders, Nucl. Phys. B 724 (2005) 247, Erratum: Nucl. Phys. B 854 (2012) 504, arXiv:hep-ph/0505042.
[74] C. Patrignani, et al., Particle Data Group, Chin. Phys. C 40 (2016) 100001.
[75] R.D. Ball, et al., NNPDF, J. High Energy Phys. 1504 (2015) 040, arXiv:1410.8849 [hep-ph].
[76] M.A. Ebert, F.J. Tackmann, J. High Energy Phys. 03 (2020) 158, arXiv:1911.08486 [hep-ph].
[77] T. Sjostrand, S. Ask, J.R. Christiansen, R. Corke, N. Desai, P. Ilten, S. Mrenna, S. Prestel, C.O. Rasmussen, P.Z. Skands, Comput. Phys. Commun. 191 (2015) 159, arXiv:1410.3012 [hep-ph].
[78] S. Frixione, B.R. Webber, J. High Energy Phys. 06 (2002) 029, arXiv:hep-ph/0204244 [hep-ph].
[79] J. Alwall, R. Frederix, S. Frixione, V. Hirschi, F. Maltoni, O. Mattelaer, H.S. Shao, T. Stelzer, P. Torrielli, M. Zaro, J. High Energy Phys. 07 (2014) 079, arXiv:1405.0301 [hep-ph].